Strain accumulation in sand due to cyclic loading: drained triaxial tests

T. Wichtmann[i)], A. Niemunis, Th. Triantafyllidis

Institute of Soil Mechanics and Foundation Engineering, Ruhr-University Bochum, Universitätsstrasse 150, 44801 Bochum, Germany

Abstract

Our aim is the prediction of the accumulation of strain and/or stress under cyclic loading with many (thousands to millions) cycles and relatively small amplitudes. A high-cycle constitutive model is used for this purpose. Its formulas are based on numerous cyclic tests. This paper describes drained tests with triaxial compression and uniaxial stress cycles. The influence of the strain amplitude, the average stress, the density, the cyclic preloading history and the grain size distribution on the direction and the intensity of strain accumulation is discussed.

Key words: Cyclic tests; Triaxial compression; Uniaxial cyclic stress paths; Accumulation; Residual strain; Explicit model; Sand

1 Introduction

Cyclic loading leads to an accumulation of strain and/or excess pore water pressures in soils because the generated stress or strain loops are not perfectly closed. Such cumulative phenomena are of importance in many practical cases. In the seismic areas a limited number of load cycles with large amplitudes (i.e. $\varepsilon^{\text{ampl}} > 10^{-3}$) during an earthquake may lead to an accumulation of high pore water pressures and consequently to a dramatic loss of the bearing capacity of structures (liquefaction). Also offshore foundations may loose their bearing capacity in a similar way during a storm. Under drained conditions if the amplitude is small (i.e. $\varepsilon^{\text{ampl}} < 10^{-3}$) and the number of cycles is high the accumulation of settlements becomes the main concern (long-term serviceability, e.g. railways, watergates, tanks). Some structures are extremely sensitive to differential settlements, which must be kept within an extremely small range in order to ensure the operational requirements. In this case an accurate prediction is required for several decades of intensive traffic.

For the finite element (FE) prediction of residual settlements two different numerical strategies can be distinguished. The *implicit* (incremental or low-cycle) models need hundreds of load increments per cycle and the residual settlement appears as a by-product of classically calculated stress - strain loops. The accumulation results from the fact that the cycles are not per-

fectly closed. The implicit approach is suitable for a relatively low number of cycles (say $N < 50$) and general purpose constitutive models can be used (usually multi-surface plasticity models, Mróz and Norris [1], Dafalias [2]).

The present research is devoted to another so-called *explicit* (high-cycle) model. In such a model only the first two cycles are calculated conventionally with strain increments (see Fig. 1). The strain amplitude is determined from the second cycle. The first, so-called *irregular* cycle is not suitable for this purpose, because it may differ significantly from the following so-called *regular* ones. The accumulation due to the following cycles is determined from a direct (explicit) formula. The material model predicts the residual strain due to a package of e.g. $\Delta N = 20$ cycles by the piece without tracing the oscillating strain path during the individual cycles. The strain amplitude is assumed to be constant during this calculation. In order to update the strain amplitude after a possible densification or re-distribution of stress, the explicit calculation can be interrupted by a so-called *control cycle* (*semi-explicit* approach). For a high number (e.g. several thousands) of cycles explicit models turn out to be more useful and accurate because the accumulation of systematic errors in implicit models is of the order of the physical accumulation.

The explicit constitutive model is based on experimental observations. We have performed numerous cyclic triaxial and cyclic multiaxial direct simple shear tests. The results of the tests with triaxial compression

---
[i)]Corresponding author. Tel.: + 49-234-3226080; fax: +49-234-3214150; *e-mail address:* torsten.wichtmann@rub.de
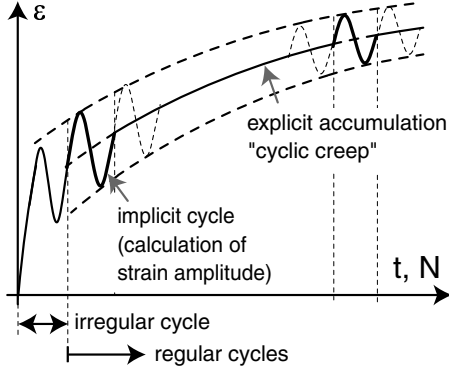
Fig. 1: Calculation procedure of explicit models

and uniaxial stress cycles are presented in this paper. The multiaxial tests are described in [3].

2   Notation, preliminaries

We use the effective Cauchy stress $\boldsymbol{\sigma}$ (compression positive) and small strain components. The Roscoe variables are

$$p = \operatorname{tr}\boldsymbol{\sigma}/3 = (\sigma_1 + 2\sigma_3)/3 \tag{1}$$

$$q = \sqrt{3/2}\,\|\boldsymbol{\sigma}^*\| = \sigma_1 - \sigma_3 \tag{2}$$

and the work conjugated strain rates are

$$\dot{\varepsilon}_v = \operatorname{tr}\dot{\boldsymbol{\varepsilon}} = \dot{\varepsilon}_1 + 2\dot{\varepsilon}_3 \tag{3}$$

$$\dot{\varepsilon}_q = \sqrt{2/3}\,\|\dot{\boldsymbol{\varepsilon}}^*\| = 2/3\,(\dot{\varepsilon}_1 - \dot{\varepsilon}_3) \tag{4}$$

The star $\sqcup^*$ designates the deviatoric part of $\sqcup$. We denote the axial component with the index $\sqcup_1$ and the radial components with $\sqcup_2$ and $\sqcup_3$. Using the word "rate" we mean the derivative with respect to the number of cycles N, that is $\dot{\sqcup} = \partial\sqcup/\partial N$ and not with respect to time.

Stress obliquity is expressed with $\eta = q/p$ or using the yield function $Y = -I_1 I_2 / I_3$ of Matsuoka and Nakai [4] as

$$\bar{Y} = \frac{Y-9}{Y_c-9} \quad \text{with} \quad Y = \frac{27(3+\eta)}{(3+2\eta)(3-\eta)} \tag{5}$$

and with $Y_c = (9 - \sin^2\varphi_c)/(1 - \sin^2\varphi_c)$. The critical friction angle is denoted by φ_c and the one at peak as φ_p. The inclinations of the critical state line (CSL, see Fig. 2) are

$$M_c = \frac{6\,\sin\varphi_c}{3-\sin\varphi_c} \quad \text{and} \quad M_e = -\frac{6\,\sin\varphi_c}{3+\sin\varphi_c} \tag{6}$$

for compression and extension corresponding both to $\bar{Y} = 1$.

In all tests the average stress $\boldsymbol{\sigma}^{\mathrm{av}}$ was kept constant and the axial stress component σ_1 was cyclically varied with an amplitude σ_1^{ampl} (see Fig. 2). It is convenient to introduce the normalized size of the stress amplitude

$$\zeta = \sigma_1^{\mathrm{ampl}}/p^{\mathrm{av}} = q^{\mathrm{ampl}}/p^{\mathrm{av}} . \tag{7}$$
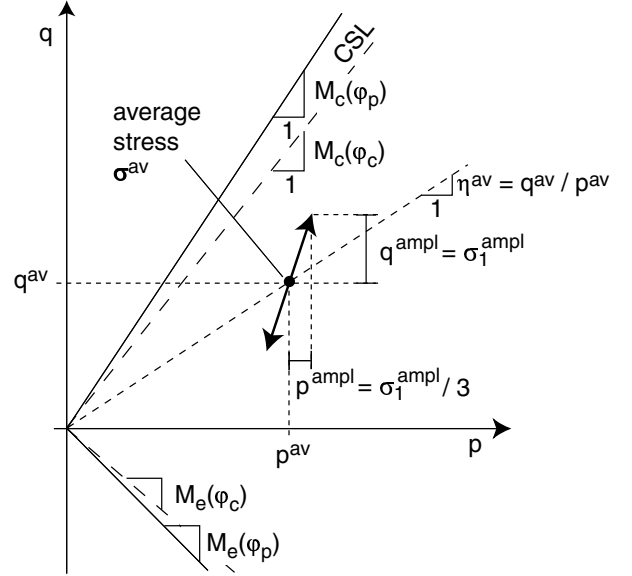
Fig. 2: State of stress in a cyclic triaxial test

The strains under cyclic loading can be decomposed into a residual and a resilient portion denoted by the superscripts $\sqcup^{\mathrm{acc}}$ and $\sqcup^{\mathrm{ampl}}$, respectively. We abbreviate the norm of the former as

$$\varepsilon^{\mathrm{acc}} = \|\boldsymbol{\varepsilon}^{\mathrm{acc}}\| = \sqrt{(\varepsilon_1^{\mathrm{acc}})^2 + 2(\varepsilon_3^{\mathrm{acc}})^2} \tag{8}$$

with the direction of strain accumulation (cyclic flow rule)

$$\omega = \varepsilon_v^{\mathrm{acc}}/\varepsilon_q^{\mathrm{acc}} . \tag{9}$$

$\varepsilon_v^{\mathrm{acc}}$ and $\varepsilon_q^{\mathrm{acc}}$ are the cumulative volumetric and deviatoric strain components, respectively. The strain amplitude generated by an uniaxial stress loop is described by

$$\varepsilon^{\mathrm{ampl}} = \|\boldsymbol{\varepsilon}^{\mathrm{ampl}}\| \tag{10}$$

or the volumetric ($\varepsilon_v^{\mathrm{ampl}}$) and deviatoric ($\varepsilon_q^{\mathrm{ampl}}$) components. Alternatively also the shear strain amplitude is used:

$$\gamma^{\mathrm{ampl}} = \sqrt{3/2}\,\|(\boldsymbol{\varepsilon}^*)^{\mathrm{ampl}}\| = (\varepsilon_1 - \varepsilon_3)^{\mathrm{ampl}} \tag{11}$$

The tests were done at various density indices $I_D = (e_{\max} - e)/(e_{\max} - e_{\min}) = D_r\,\varrho_{d,max}/\varrho_d$ (D_r = relative density, ϱ_d = dry density).

3 Need for a systematic study

Most of the studies on the cyclic behaviour of sand concern a low number of cycles (e.g. $N < 1,000$) and it is unclear, if the observations can be extended to the high-cycle behaviour. The few studies going beyond $N = 1,000$ are either not well documented (e.g. the strain amplitudes are not available) or their testing program is incomplete. Some of the published results are contradictory.

There is a general consent that with increasing number of cycles N the residual strain $\varepsilon^{\mathrm{acc}}$ increases without a clear limit while the rate of accumulation $\dot{\varepsilon}^{\mathrm{acc}}$ decreases. Different approximations of the experimental curves $\varepsilon^{\mathrm{acc}}(N)$, however, were proposed. In cyclic triaxial tests Lentz and Baladi [5,6] observed the increase of the residual vertical strain $\varepsilon_1^{\mathrm{acc}}$ to be proportional to the logarithm of the number of cycles N. Similarly Suiker [7] found from cyclic triaxial tests on gravel and sand that the accumulation rate $\dot{\varepsilon}^{\mathrm{acc}}$ decreases proportional to $1/N$, however, with two proportionality coefficients c_1 for $N < 1,000$ and c_2 for $N > 1,000$ with $c_1 > c_2$. Helm et al. [8] observed similar proportionality coefficients but with $c_2 > c_1$ (cyclic triaxial tests on medium coarse and fine sand). An accumulation faster than the logarithm of the number of cycles was also observed by Gotschol [9] in cyclic triaxial tests on gravel.

The effect of the strain amplitude was mainly studied in direct simple shear (DSS) tests. Youd [10] reported a considerable increase of the rate of accumulation with increasing shear strain amplitude γ^{ampl}. For amplitudes $\gamma^{\mathrm{ampl}} < 10^{-4}$, however, he observed no accumulation of residual strain. Similar experimental results were obtained by Silver and Seed [11]. Sawicki and Świdziński [12,13] performed DSS tests with different shear strain amplitudes. For a given initial density they demonstrated a unique curve $\varepsilon_v^{\mathrm{acc}} = C_1 \, \ln(1 + C_2 \tilde{N})$ (which they called "common compaction curve") wherein $\tilde{N} = N \, (\gamma^{\mathrm{ampl}}/2)^2$. These test results may be affected by the disadvantages of DSS tests, namely the inhomogeneous distribution of strain over the specimen volume and the accumulation of lateral stresses, which are usually not measured (c.f. Budhu [14]). Furthermore, the applied number of cycles was rather small in all these tests. The common compaction curve was not confirmed by our triaxial tests with a large number of cycles, see Section 6. From cyclic triaxial tests performed by Marr and Christian [15] one could conclude a relationship $\dot{\varepsilon}^{\mathrm{acc}} \sim (\sigma_1^{\mathrm{ampl}})^b$ with the exponent b in the range $1.91 \le b \le 2.32$. Marr and Christian [15] provided data up to 10,000 cycles.

In the above mentioned studies only *deviatoric* or predominant deviatoric strain amplitudes were applied. Ko and Scott [16] performed complementary tests (on cubical specimens) using isotropic stress amplitudes. After a small initial compaction no further accumulation was observed. Ko and Scott [16] suggested to neglect the effect of the volumetric amplitude on the accumulation rate. Experiments of Wichtmann et al. [3] have demonstrated this false. The volumetric strain amplitude does affect the accumulation, although not as strongly as the deviatoric component. The influence of the space encompassed by the strain loop and its polarization (Pyke et al. [17], Ishihara and Yamazaki [18], Yamada and Ishihara [19], Wichtmann et al. [3]) has been reported elsewhere.

Several experimental studies with cyclic simple shear tests (e.g. Silver and Seed [11], Youd [10], Sawicki and Świdziński [12]) ended with the conclusion that the average mean pressure p^{av} does not influence the accumulation of residual strain. Our own tests, Section 7, show a *significant* influence of the average stress. Marr and Christian [15] observed a slightly higher accumulation rate at a higher p^{av} (keeping $\zeta = \sigma_1^{\mathrm{ampl}}/p^{\mathrm{av}}$ constant) and an increase of the accumulation rate with the average stress ratio η^{av}. However, the different strain amplitudes in the tests due to the stress-dependence of the stiffness were not taken into account (the strain amplitudes may differ significantly with p^{av} or η^{av}, see Figs. 11 and 15).

From numerous cyclic simple shear tests (e.g. Silver and Seed [11], Youd [10]) and cyclic triaxial tests (e.g. Marr and Christian [15]) it is evident that the initial soil density is an important parameter for the prediction of accumulation.

The influence of the frequency of cyclic loading on the accumulation rate was found to be negligible in some studies (Youd [10] for $0.2 \le f \le 1.9$ Hz, Shenton [20] for $0.1 \le f \le 30$ Hz) and to be significant in others (Kempfert et al. [21]).

The *direction* of accumulation (cyclic flow rule) was studied by Luong [22] in drained cyclic triaxial tests. Small packages with 20 load cycles were applied successively to the same sand specimen. The average stress was varied from package to package and the accumulated strain was monitored. The so-called "characteristic threshold" (CT) line in the p - q - plane was postulated such that $\boldsymbol{\sigma}^{\mathrm{av}}$ below the CT line leads to densification and $\boldsymbol{\sigma}^{\mathrm{av}}$ above the CT line to dilative accumulation. Chang and Whitman [23] found that the direction of accumulation could be well expressed using the flow rule of the modified Cam Clay model $\omega = (M_c^{\,2} - (\eta^{\mathrm{av}})^2)/(2\eta^{\mathrm{av}})$. They proposed to identify Luong's CT line with the critical state line (CSL). The CT line was shown to be independent of p^{av}, of the stress amplitude and the density. However, no experimental data for the cyclic flow rule for $N > 1,050$ was presented. We investigated whether the slight increase of ω with N in the diagrams of Chang and Whitman

[23] continues beyond $N > 1,050$.

4   Testing device, preparation of samples and tested materials
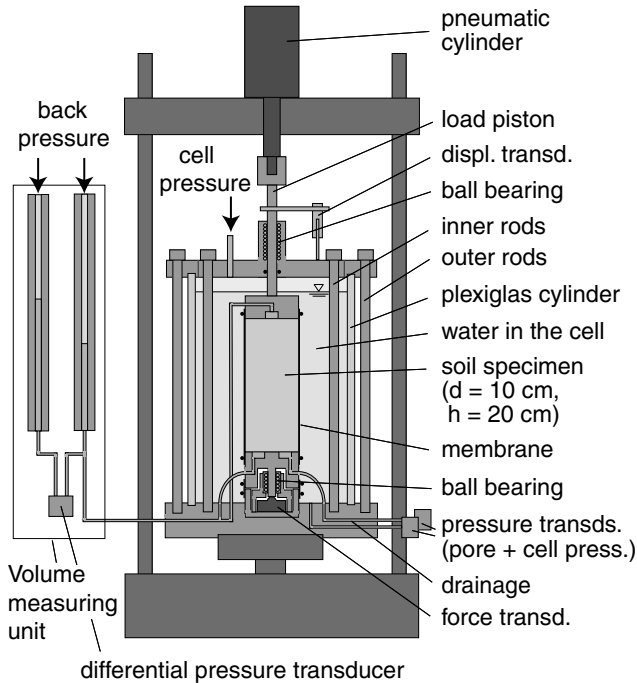
Fig. 3: Scheme of cyclic triaxial test device

In our study we used five triaxial devices of the type presented in Fig. 3. The axial load was applied by a pneumatic loading system and measured at a load cell inside the pressure cell below the lower specimen end plate. The axial deformation of the specimen was monitored by a displacement transducer of a high accuracy which was fixed to the load piston. Due to the smearing of the end plates the bedding error was carefully subtracted. The inhomogeneity of the resilient and the cumulative deformation in a triaxial sample was investigated by Niemunis [24] using the PIV-technique. These inhomogeneities remain even after a large number of cycles, both in the amplitude and in the accumulation rate. Local axial strain measurements with a short distance ($<$ 5 cm) between the reference points can therefore lead to errors. The integral value of the whole sample is thought to be more representative (although there may be some disturbance at the top of the sample).

For technical reasons it was easier to perform tests with saturated specimens than with dry ones. The results do not differ significantly. The volume changes of fully saturated specimens were measured by the squeezed out pore water using a differential pressure transducer. The lateral deformations of the dry specimens were determined with six local non-contact displacement transducers (LDT) distributed over the specimen surface.

Cell pressure and back pressure were monitored by means of pressure transducers.

Specimens were prepared by pluviating dry sand out of a funnel through air into half-cylinder moulds. The funnel was being lifted so that the drop height was kept constant. Different initial densities were achieved by varying the outlet diameter of the funnel. If the specimen was supposed to be water-saturated it was first flushed with carbon dioxide and then saturated with de-aired water. Back pressures of 200 or 300 kPa were used. The quality of saturation was approved if B > 0.95 (B = parameter of Skempton).

Starting from a small isotropic effective stress, the cell pressure was isotropically increased to σ_3^{av} and then the axial stress was raised to σ_1^{av}. During the application of $\boldsymbol{\sigma}^{\mathrm{av}}$ the deformations were continuously measured. The cyclic loading with σ_1^{ampl} was commenced after a one-hour consolidation period at $\boldsymbol{\sigma}^{\mathrm{av}}$. In all tests (except those on the influence of the loading frequency, Section 9) the specimens were subject to 10^5 cycles at a frequency of 1 Hz. The signals of all transducers were recorded over the period of five complete cycles after an idle (non-recording) phase of ΔN cycles. The gaps ΔN between the readings were inversely proportional to the accumulation rate (increase with N).
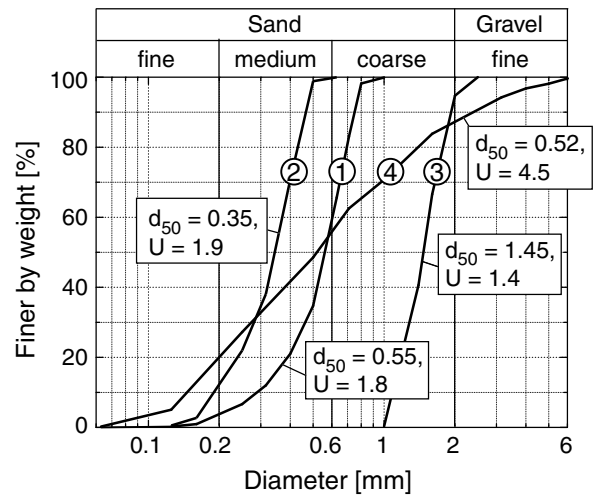
Fig. 4: Tested grain size distribution curves (d_{50}: mean grain diameter, $U = d_{60}/d_{10}$: uniformity index)

This experimental study was performed with a quartz sand with subrounded grains. In all tests except those on the influence of the grain size distribution (see Section 11) the sieve curve No. 1 in Fig. 4 with the minimum and maximum void ratios $e_{\min} = 0.577$ and $e_{\max} = 0.874$ (German standard code DIN 18126) and a critical friction angle $\varphi_c = 31.2°$ was used.

5 The high-cycle accumulation model

In this section the explicit accumulation model (see Niemunis et al. [25]) is briefly presented. The general stress-strain relation has the form

$$\dot{\boldsymbol{\sigma}} \;=\; \mathsf{E} : (\dot{\boldsymbol{\varepsilon}} - \dot{\boldsymbol{\varepsilon}}^{\mathrm{acc}}) \tag{12}$$

wherein E denotes an elastic stiffness. The rate of strain accumulation $\dot{\boldsymbol{\varepsilon}}^{\mathrm{acc}}$ is proposed to be

$$\dot{\boldsymbol{\varepsilon}}^{\mathrm{acc}} \;=\; \dot{\varepsilon}^{\mathrm{acc}}\, \mathbf{m} \tag{13}$$
$$= \; f_p\, f_Y\, f_e\, f_\pi\, (\underbrace{f_{\mathrm{ampl}}\, \dot{f}_N^A}_{\dot{g}^A} + \underbrace{f_{\mathrm{ampl}}\, \dot{f}_N^B}_{\dot{g}^B})\, \mathbf{m}$$

with the direction expressed by the unit tensor $\mathbf{m}$ (for triaxial tests $\omega = \sqrt{3/2}\,\mathrm{tr}\,(\mathbf{m})/\|\mathbf{m}^*\|$ holds) and with the intensity $\dot{\varepsilon}^{\mathrm{acc}} = \|\dot{\boldsymbol{\varepsilon}}^{\mathrm{acc}}\|$. While the cyclic flow rule $\mathbf{m}$ is a function of the average stress ratio $\eta^{\mathrm{av}} = q^{\mathrm{av}}/p^{\mathrm{av}}$ only, the intensity of strain accumulation $\dot{\varepsilon}^{\mathrm{acc}}$ depends on the amplitude, the shape and the polarization of the strain loop, the average stress $\boldsymbol{\sigma}^{\mathrm{av}}$, the void ratio e and the applied number of cycles N, i.e. the cyclic preloading history. In the proposed expression (13) the respective functions describe the following contributions:

f_{ampl}: amplitude, shape and polarization of the strain loop, summarized in the scalar $\varepsilon^{\mathrm{ampl}}$
f_p: average mean stress p^{av}
f_Y: average stress ratio $\bar{Y}^{\mathrm{av}}$
f_e: average void ratio e
$\dot{f}_N^A,\, \dot{f}_N^B$: cyclic preloading
= number of cycles N, if $\varepsilon^{\mathrm{ampl}}$ = constant
f_π: polarization changes

These functions (except f_π) and the cyclic flow rule $\mathbf{m}$ were derived on the basis of the performed cyclic triaxial tests and are discussed in the following sections, see also Table 1.

The number of cycles N is not a suitable state variable for cyclic preloading since it contains no information about the amplitude of the previous cycles. Thus, a new state variable $g^A = \int \dot{g}^A\, \mathrm{d}N = \int f_{\mathrm{ampl}}\, \dot{f}_N^A\, \mathrm{d}N$ was introduced which considers both N and $\varepsilon^{\mathrm{ampl}}$ in the past.

In this paper only the special case of a one-dimensional cyclic strain path is studied. In order to capture more complex strain loops the accumulation model uses a tensorial amplitude definition (see Niemunis [24] or Niemunis et al. [25]). For a one-dimensional strain loop, however, this new amplitude definition is identical to the classical one.

The function f_π was determined from cyclic multiaxial direct simple shear (CMDSS) tests and is presented elsewhere (Wichtmann et al. [3]). For the case that the polarization of the strain loop does not change during cyclic loading (e.g. in the performed cyclic triaxial tests) $f_\pi = 1$ holds.

Function	Mat. constants	
$f_{\mathrm{ampl}} = \left(\varepsilon^{\mathrm{ampl}}/\varepsilon_{\mathrm{ref}}^{\mathrm{ampl}}\right)^2$	$\varepsilon_{\mathrm{ref}}^{\mathrm{ampl}}$	10^{-4}
$\dot{f}_N^A = C_{N1} C_{N2} \exp\left(-\dfrac{g^A}{C_{N1}\, f_{\mathrm{ampl}}}\right)$	C_{N1}	$3.4 \cdot 10^{-4}$
$\dot{f}_N^B = C_{N1} C_{N3}$	C_{N2}	0.55
	C_{N3}	$6.0 \cdot 10^{-5}$
$f_p = \exp\left[-C_p\left(\dfrac{p^{\mathrm{av}}}{p_{\mathrm{ref}}} - 1\right)\right]$	C_p	0.43
	p_{ref}	100 kPa
$f_Y = \exp\left(C_Y\, \bar{Y}^{\mathrm{av}}\right)$	C_Y	2.0
$f_e = \dfrac{(C_e - e)^2}{1 + e}\, \dfrac{1 + e_{\mathrm{ref}}}{(C_e - e_{\mathrm{ref}})^2}$	C_e	0.54
	e_{ref}	0.874
$f_\pi = 1$ if polarization = constant, else see Wichtmann et al. [3]		

Table 1: Summary of the partial functions f_i and a list of the material constants C_i for the tested sand

6 Influence of the strain amplitude

The effect of the strain amplitude $\varepsilon^{\mathrm{ampl}}$ on the accumulation rate was studied in a series of tests with stress amplitudes varying between $0.06 \leq \zeta \leq 0.47$ (12 kPa $\leq q^{\mathrm{ampl}} \leq 94$ kPa). The average stress was $p^{\mathrm{av}} = 200$ kPa, $\eta^{\mathrm{av}} = 0.75$ in all tests and the initial relative density lay within $0.55 \leq I_{D0} \leq 0.64$, wherein "initial" means after the irregular cycle. Specimens were tested in the dry condition.

Keeping $\zeta(N)$ constant a decrease of the strain amplitude $\varepsilon^{\mathrm{ampl}}$ with N was noticed (Fig. 5), especially for larger amplitudes and during the first 100 cycles (so-called *conditioning phase*).

Fig. 6 presents the resulting accumulation curves $\varepsilon^{\mathrm{acc}}(N)$ in a semi-logarithmical diagram. Only the accumulation during the regular cycles is of interest and the diagrams in this paper show only this portion. The accumulated strain was found to increase almost proportionally with the logarithm of the number of cycles up to $N \approx 10,000$ and then over-proportionally. The approximation of these curves by the functions $\dot{f}_N^A$ and $\dot{f}_N^B$ is discussed in Section 10. From Fig. 6 it is obvious that higher amplitudes cause larger accumulation rates $\dot{\varepsilon}^{\mathrm{acc}}$.

In Fig. 7 the accumulated strain after different num-
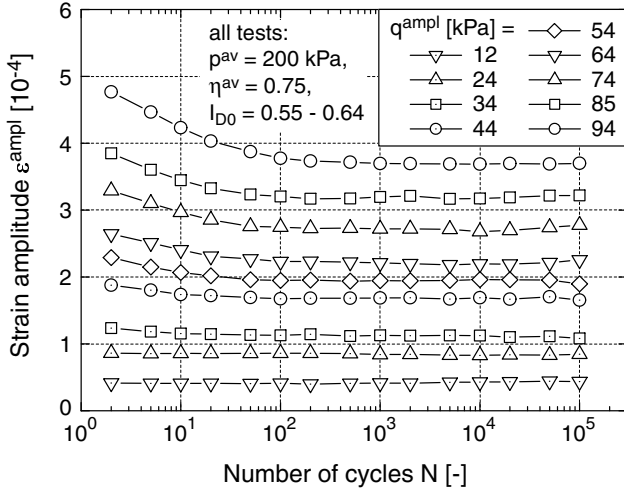
Fig. 5: Strain amplitude $\varepsilon^{\mathrm{ampl}}$ versus the number of cycles N
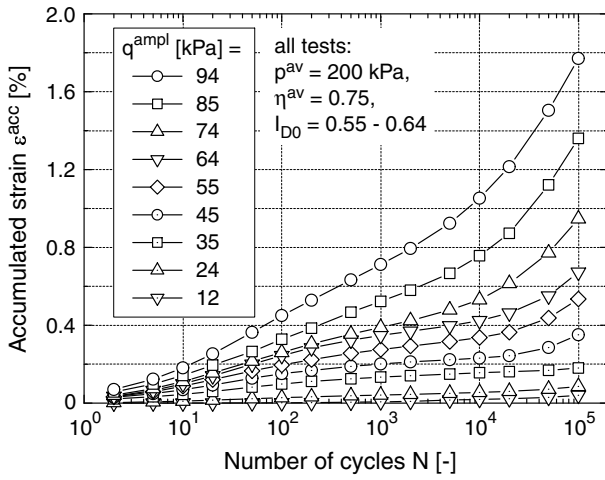
Fig. 6: Accumulation curves $\varepsilon^{\mathrm{acc}}(N)$ in tests with different stress amplitudes q^{ampl}

exponents that have been determined from the tests of Marr and Christian [15] in terms of stress amplitudes.
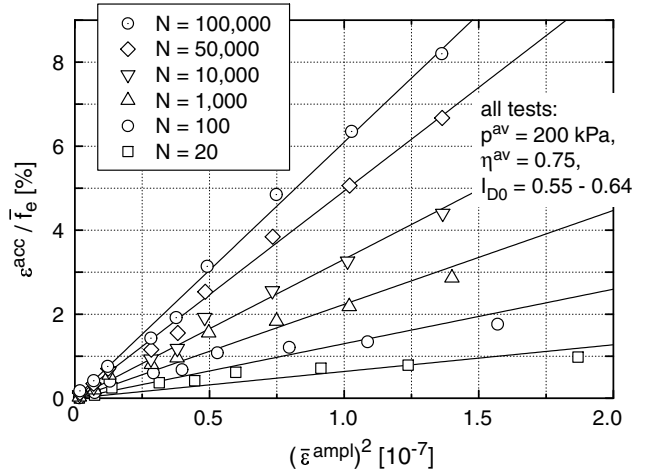
Fig. 7: Accumulated strain $\varepsilon^{\mathrm{acc}}/\bar{f}_e$ as a function of the square of the strain amplitude $(\bar{\varepsilon}^{\mathrm{ampl}})^2$
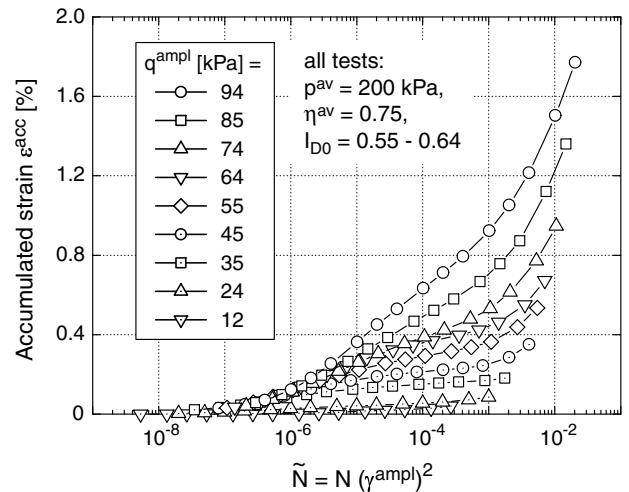
Fig. 8: Accumulated strain $\varepsilon^{\mathrm{acc}}$ in dependence on $\tilde{N} = N\,(\gamma^{\mathrm{ampl}})^2$ as proposed by Sawicki and Świdziński [12,13]

bers of cycles is plotted versus the square of the strain amplitude. Since $\varepsilon^{\mathrm{ampl}}$ varies slightly with N (Fig. 5) the mean value $\bar{\varepsilon}^{\mathrm{ampl}} = (\int_1^N \varepsilon^{\mathrm{ampl}}\,\mathrm{d}N)/N$ is used in Fig. 7. The accumulated strain $\varepsilon^{\mathrm{acc}}$ is normalized with the void ratio function f_e (Section 8) in order to remove the effect of the slightly varying initial densities and the different compaction rates in the nine tests. The bar over f_e means that f_e is calculated with a mean value of the void ratio $\bar{e} = (\int_1^N e\,\mathrm{d}N)/N$. The curves in Fig. 7 reveal that the accumulation rate $\dot{\varepsilon}^{\mathrm{acc}}$ increases proportionally to $(\varepsilon^{\mathrm{ampl}})^2$, independently of N. The following amplitude function

$$ f_{\mathrm{ampl}} = \left(\frac{\varepsilon^{\mathrm{ampl}}}{\varepsilon^{\mathrm{ampl}}_{\mathrm{ref}}} \right)^2 \qquad (14) $$

is therefore proposed wherein the reference amplitude is $\varepsilon^{\mathrm{ampl}}_{\mathrm{ref}} = 10^{-4}$. Function (14) is in agreement with the

In Fig. 8 the accumulated strain is shown as a function of $\tilde{N} = N\,(\gamma^{\mathrm{ampl}})^2$ and according to the "common compaction curve" proposed by Sawicki and Świdziński [12,13] the curves $\varepsilon^{\mathrm{acc}}(\tilde{N})$ should coincide. Evidently, they do not.

Fig. 9 presents the strain ratio ω as a function of the strain amplitude $\varepsilon^{\mathrm{ampl}}$. At higher values of $\varepsilon^{\mathrm{ampl}}$ the strain ratio is almost independent of $\varepsilon^{\mathrm{ampl}}$. At smaller strain amplitudes the accumulated volumetric and deviatoric strains were very small and therefore the values of ω could be inaccurate. Thus the direction of accumulation is thought to be independent of the strain amplitude. This is in accordance with the experimental results of Chang and Whitman [23] for lower cycle numbers. Plots of ω over N demonstrate an increase of

the volumetric component of the direction of accumulation with the number of cycles.
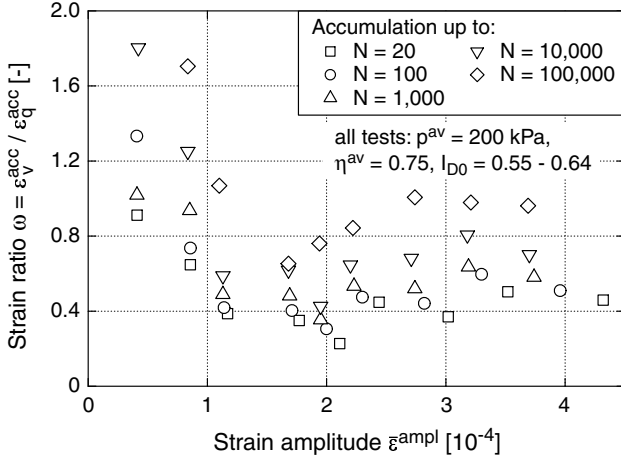
Fig. 9: Strain ratio ω as a function of the strain amplitude $\varepsilon^{\mathrm{ampl}}$

7   Influence of the average stress

The average stress was varied between 50 kPa $\leq p^{\mathrm{av}} \leq$ 300 kPa and $0.25 \leq \eta^{\mathrm{av}} = q^{\mathrm{av}}/p^{\mathrm{av}} \leq 1.375$ keeping $\zeta = 0.3$ constant. Specimens were prepared with the initial densities $0.57 \leq I_{D0} \leq 0.69$ and tested in the saturated condition. The obtained results contradict the assumption made by several researchers (Silver and Seed [11], Youd [10], Sawicki and Świdziński [12]), that the average stress does not influence the accumulation process.
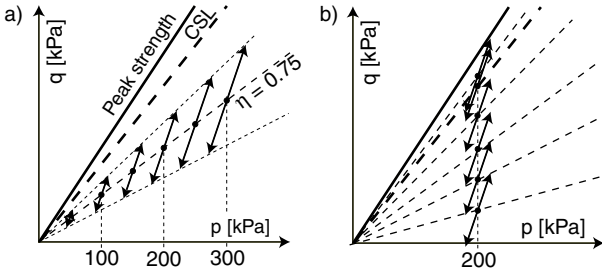
Fig. 10: Stress paths in tests on the influence of the average stress, a) variation of p^{av}, b) variation of η^{av}

The cyclic stress paths of a series of six tests with an identical average stress ratio ($\eta^{\mathrm{av}} = 0.75$) but different average mean pressures are presented in Fig. 10a. Figs. 11 - 14 contain the results of these tests. The strain amplitudes slightly increased with increasing average mean pressure (Fig. 11) due to the well known dependence of stiffness $G \sim p^n$ (here: $n = 0.75$), i.e. slightly underproportional to p.

Fig. 12 presents the accumulated strain as a function of the average mean pressure p^{av} for different numbers
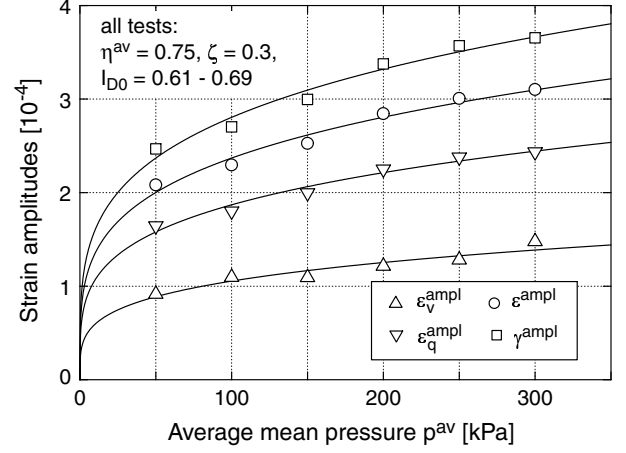
Fig. 11: Strain amplitudes in tests with different average mean pressures p^{av} but $\zeta = \mathrm{const}$ (mean values during 10^5 cycles)
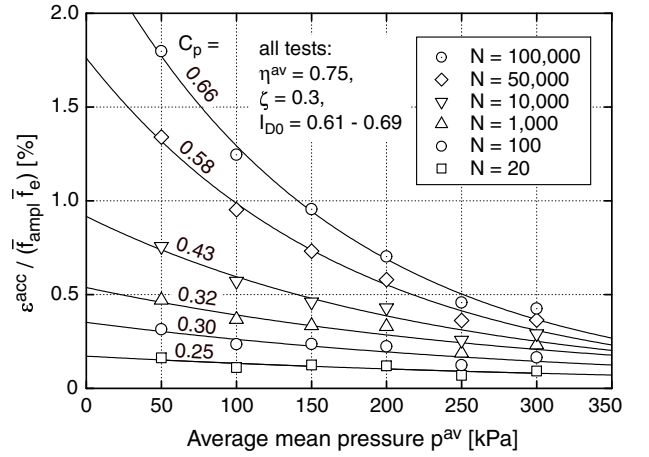
Fig. 12: Accumulated strain $\varepsilon^{\mathrm{acc}}/(\bar{f}_{\mathrm{ampl}} \, \bar{f}_e)$ in dependence on the average mean pressure p^{av}

of cycles. For comparison the residual strain has been purified from side effects, i.e. divided by the amplitude function f_{ampl} and by the void ratio function f_e. It was interesting to observe that the accumulated strain significantly increases with decreasing (!) average mean pressure. This pressure dependence is stronger for large N. The function f_p is proposed in the simple form

$$f_p = \exp\left[-C_p \left(\frac{p^{\mathrm{av}}}{p_{\mathrm{ref}}} - 1\right)\right]. \qquad (15)$$

The atmospheric pressure $p_{\mathrm{ref}} = p_{\mathrm{atm}} = 100$ kPa is used as a reference for which $f_p = 1$ holds. Equation (15) has been confirmed by the data in Fig. 12 for different numbers of cycles. The corresponding curves are shown as solid lines in Fig. 12 and the parameter C_p is given at each curve. C_p turns out to increase with N. However, in order to keep the number of material constants manageable, a constant mean value of $C_p = 0.43$

is proposed. The diagram in Fig. 13 is similar to that in Fig. 12 with the only difference, that the dependencies on $\bar{Y}^{\mathrm{av}}$ (see remarks later in this Section) and N (see Section 10) have been removed. The curve resulting from equation (15) with $C_p = 0.43$ in Fig. 13 demonstrates, that the loss of accuracy due to the assumption $C_p = \mathrm{const}$ is acceptable.
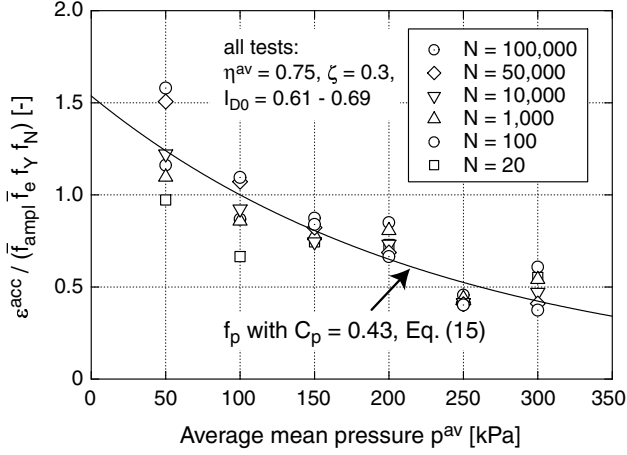
Fig. 13: Accumulated strain $\varepsilon^{\mathrm{acc}}/(\bar{f}_{\mathrm{ampl}}\,\bar{f}_e\,f_Y\,f_N)$ in dependence on the average mean pressure p^{av}

The direction of accumulation was found to be relatively insensitive to changes in the average mean pressure (Fig. 14). A slight increase of the strain ratio ω with a decreasing average mean pressure and with N could be observed. The increase with N was observed for dry (Fig. 9) and for fully saturated specimens (Fig. 14).
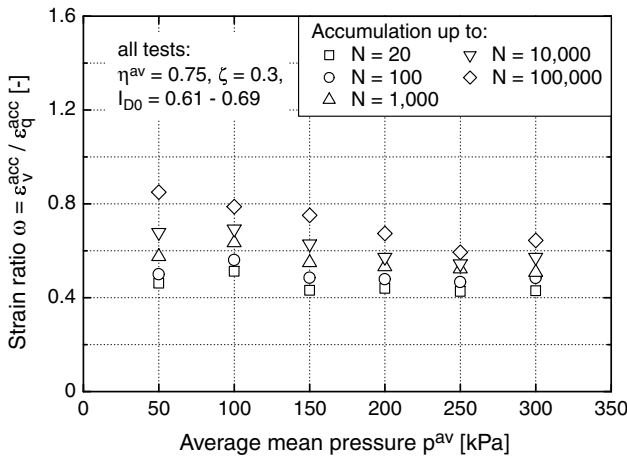
Fig. 14: Strain ratio ω as a function of the average mean pressure p^{av}

The results of a series of eleven tests with $0.375 \leq \eta^{\mathrm{av}} \leq 1.375$ ($0.088 \leq \bar{Y}^{\mathrm{av}} \leq 1.243$) and $p^{\mathrm{av}} = 200$ kPa $= \mathrm{const}$ and $\zeta = \mathrm{const}$ (see the scheme of the stress paths in Fig. 10b) are presented in Figs. 15 - 17.
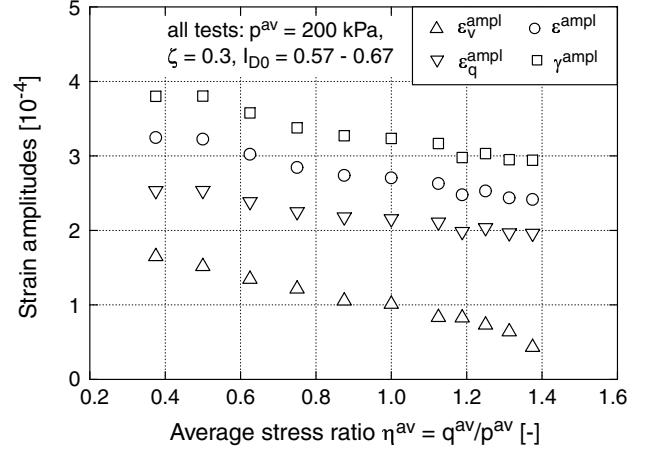
Fig. 15: Strain amplitudes in tests with different average stress ratios η^{av} (mean values during 10^5 cycles)
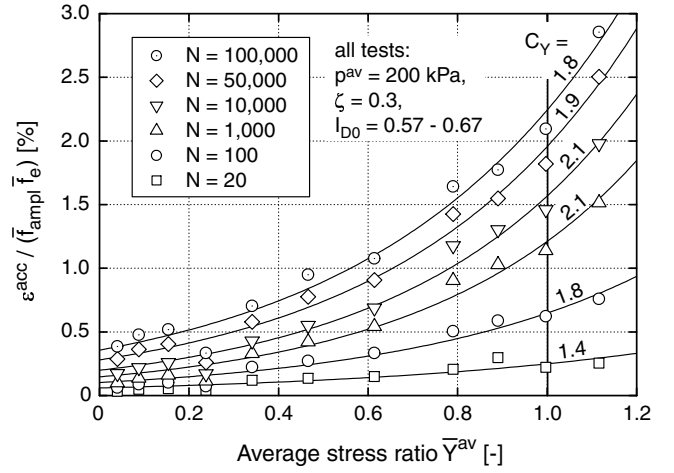
Fig. 16: Accumulated strain $\varepsilon^{\mathrm{acc}}/(\bar{f}_{\mathrm{ampl}}\,\bar{f}_e)$ in dependence on the average stress ratio $\bar{Y}^{\mathrm{av}}$

The strain amplitudes slightly decrease with increasing η^{av} as shown in Fig. 15. The accumulation increases with $\bar{Y}^{\mathrm{av}}$, Fig. 16. In the test with $\bar{Y}^{\mathrm{av}} = 1.243$ ($\eta = 1.375$) the stress cycles touched the failure line $M_c(\varphi_p)$ and the rate of accumulation exploded reaching nearly 20 % residual strain after 10^5 cycles. If the stress cycles do not surpass this limit the function f_Y can be quite well approximated by

$$f_Y \;=\; \exp\left(C_Y\,\bar{Y}^{\mathrm{av}}\right) \qquad (16)$$

The material constant $C_Y = 2.0$ is approximately independent of the number of cycles (Fig. 16). For isotropic stresses ($\bar{Y}^{\mathrm{av}} = 0$) $f_Y = 1$ holds.

Fig. 17 shows the strain ratio ω plotted versus η^{av}. A decrease of ω with η^{av} is evident. The critical stress ratio $M_c(\varphi_c) = 1.25$ was determined from static tests. It coincides with a purely deviatoric accumulation. For $\eta^{\mathrm{av}} < M_c(\varphi_c)$ densification and above the critical state
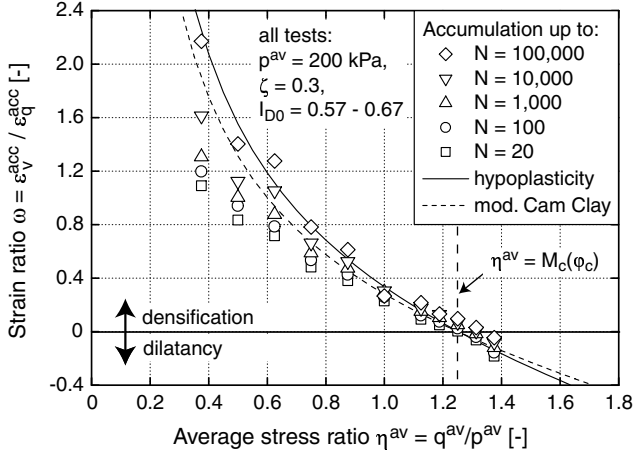
Fig. 17: Strain ratio ω as a function of average stress ratio η^{av}

line a dilative behaviour was observed. This is in accordance with the experimental results of Luong [22] and Chang and Whitman [23]. The dependence $\omega(\eta^{av})$ conforms with the flow rule of the modified Cam Clay model, as already observed by Chang and Whitman [23], or with the hypoplastic theory, Niemunis [24], Fig. 17. Both flow rules (for monotonous loading) describe well the direction of accumulation observed in the cyclic triaxial tests, especially for the higher numbers of cycles, e.g. $N = 10^5$.

Next, Fig. 18, average mean pressures $p^{av} = 100$ kPa and $p^{av} = 300$ kPa and different stress ratios $\eta^{av} > 0$ ($\zeta = 0.3 = $ const) were tested in order to study if a more complex description than $f_p\, f_Y$ is needed. Fig. 18 confirms, that the accumulation increases with *decreasing* average mean pressure p^{av} and increasing deviatoric stress ratio $\bar{Y}^{av}$. For $p^{av} = 100$, 200 and 300 kPa the same approximation (16) could be used with $C_Y = 2.0$. Analogously to Fig. 12, the parameter C_p of Eq. (15) increases with N for all tested average stress ratios η^{av} and took values $0.25 \leq C_p(N = 10^5) \leq 0.66$. Therefore, strictly speaking, C_p is not a constant. It has local extremes for $\eta^{av} = 0.75$ (maximum) and $\eta^{av} = 0.25$ (minimum). For simplicity we disregard the variability of C_p with N and η^{av} in the accumulation model.

Fig. 19 presents curves of identical residual strains after $N = 10^5$ cycles with $\varepsilon^{ampl} = 3 \cdot 10^{-4}$ and $I_{D0} = 0.60$. In a wide p-q-range the curves $\varepsilon^{acc} = $ const are almost parallel to the maximum shear strength inclination $\eta = M_c(\varphi_p)$.

The direction of accumulation at different average stresses $\boldsymbol{\sigma}^{av}$ is shown in Fig. 20. It is depicted as a unit vector starting at (p^{av}, q^{av}) and having the inclination $\varepsilon_q^{acc}/\varepsilon_v^{acc}$ towards the p-axis.
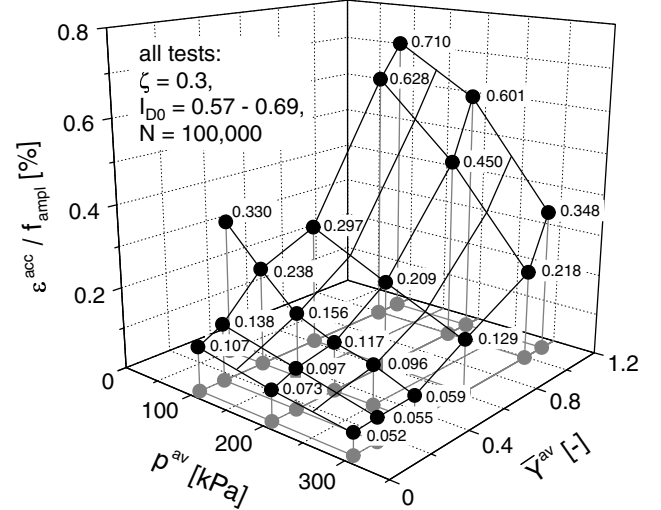
Fig. 18: Accumulated strain ε^{acc} after 100,000 load cycles for different average stresses $\boldsymbol{\sigma}^{av}$
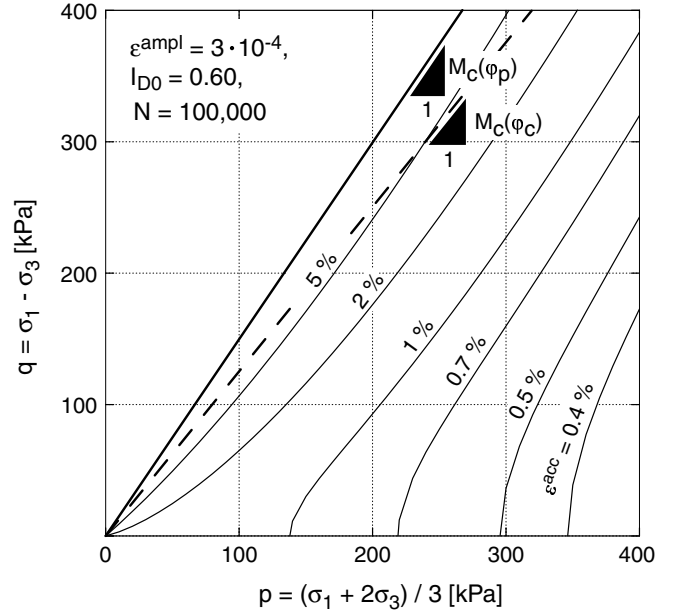
Fig. 19: Curves of identical accumulation in the p-q-plane

8 Influence of the density

In another series of tests the initial void ratio was varied between $0.58 \leq e_0 \leq 0.80$ ($0.24 \leq I_{D0} \leq 0.99$). The average stress ($p^{av} = 200$ kPa, $\eta^{av} = 0.75$) and the amplitude ratio ($\zeta = 0.3$) were kept constant this time. The specimens were water-saturated.

The condition $\zeta = q^{ampl}/p^{av} = $ const implies slightly higher strain amplitudes for lower initial densities (Fig. 21), because the stiffness decreases with the void ratio e. As it could be expected, the strain accumulation is larger in loose soils (Fig. 22). The following
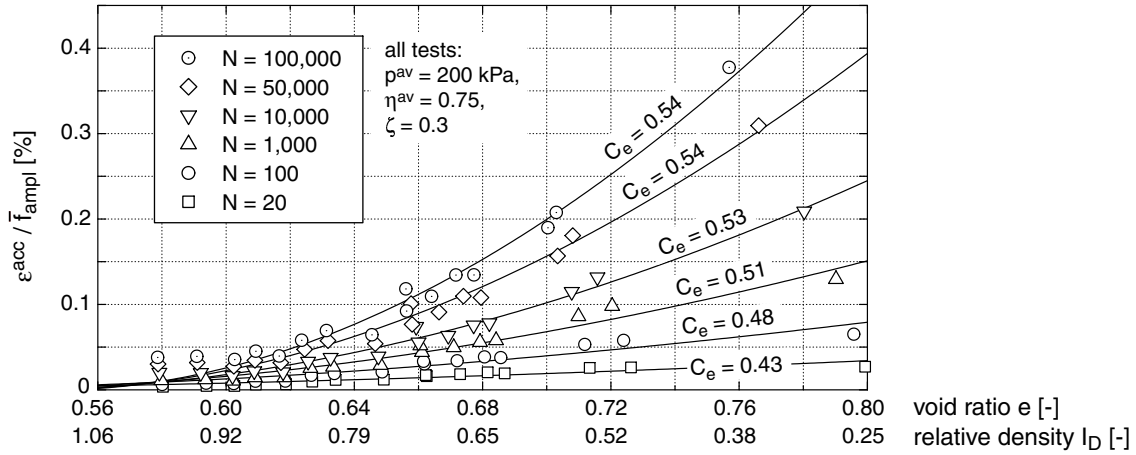
Fig. 22: *Accumulated strain $\varepsilon^{\mathrm{acc}}/\bar{f}_{ampl}$ in dependence on the void ratio e or the relative density index I_D, respectively*
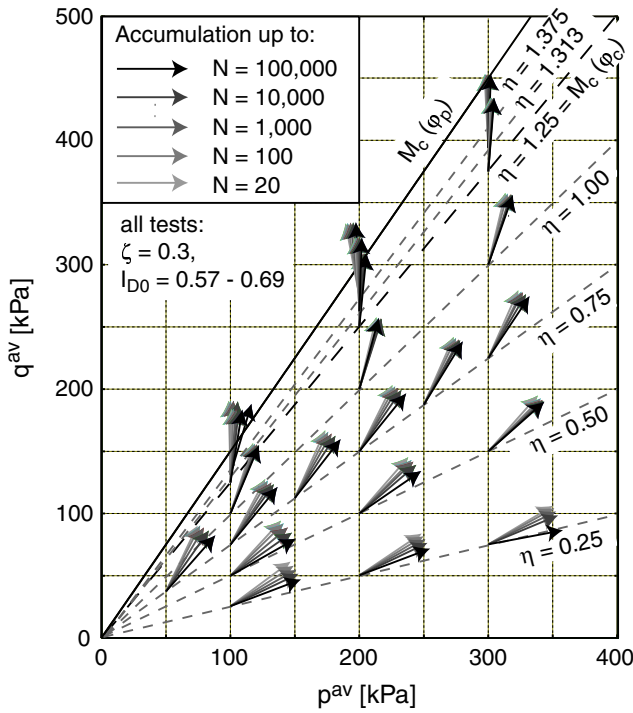
Fig. 20: Direction of accumulation in the p-q-plane for different average stresses

Fig. 21: Strain amplitudes in tests with different initial void ratios e_0 (mean values during 10^5 cycles)
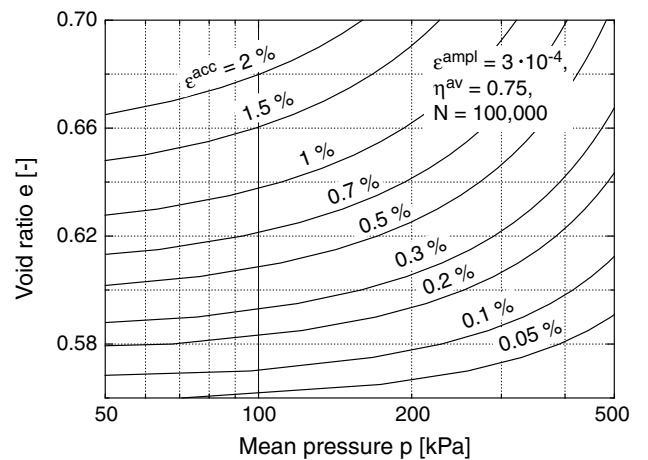
Fig. 23: Curves of identical accumulation in the e-$\ln(p)$-diagram

function was found to describe this dependence:

$$f_e \;\; = \;\; \frac{(C_e - e)^2}{1 + e} \; \frac{1 + e_{\mathrm{ref}}}{(C_e - e_{\mathrm{ref}})^2} \; . \qquad (17)$$

The material constant $C_e = 0.54$ (= void ratio for which $\dot{\varepsilon}^{\mathrm{acc}} = 0$ holds) is approximately independent of the number of cycles (Fig. 22). The reference void ratio corresponding to $f_e = 1$ is chosen to be $e_{\mathrm{ref}} = e_{\max} = 0.874$.

In Fig. 23 curves of identical accumulation $\varepsilon^{\mathrm{acc}} =$ const are plotted in the e-$\ln(p)$-diagram for $N = 10^5$,

$\varepsilon^{\mathrm{ampl}} = 3 \cdot 10^{-4}$ and $I_{D0} = 0.60$. From Fig. 23 it is obvious that the rising inclination of the curves with $\varepsilon^{\mathrm{acc}} = \mathrm{const}$ is opposite to the inclination of the critical state line. Therefore, it does not seem possible to describe the accumulation rate by the distance $e - e_c$ of the void ratio from the CSL.

The direction of accumulation was found to be independent of the void ratio for the range of densities studied (Fig. 24). However, for dense specimens ($I_{D0} > 0.90$) the scatter in the strain ratios ω was considerable (Fig. 24), probably because ω was calculated as a quotient of very small values (the accumulation was extremely slow).
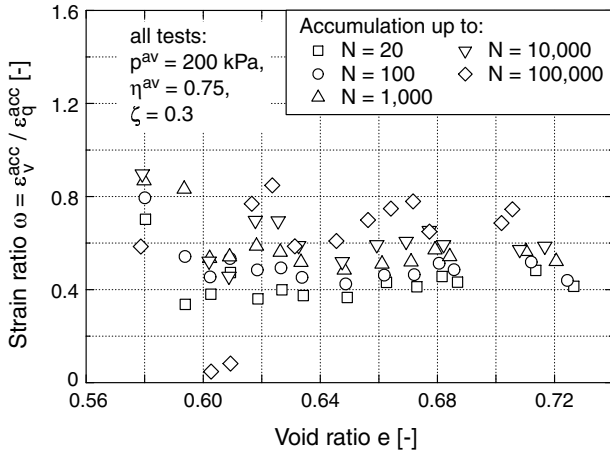
Fig. 24: Strain ratio ω as a function of the void ratio e

9   Influence of the loading frequency

In order to study the effect of the loading frequency six tests with $p^{\mathrm{av}} = 200$ kPa, $\eta^{\mathrm{av}} = 0.75$, $\zeta = 0.3$, $0.50 \leq I_{D0} \leq 0.60$ and varying loading frequencies 0.05 Hz $\leq f \leq 2$ Hz were carried out.

The loading frequency has almost no effect on the strain amplitudes, Fig. 25. The residual strains presented in Fig. 26 exhibit no dependence on the loading frequency. The direction of accumulation is also independent of f (Fig. 27). These observations coincide with the work of Youd [10] and Shenton [20] but contradict the results of Kempfert et al. [21].

10   Influence of the number of cycles

The accumulation curves $\varepsilon^{\mathrm{acc}}(N)$ normalized by f_{ampl}, f_p, f_Y, f_e and f_π with $f_\pi = 1$ are shown in Fig. 28. The curves lie within a band, which can be approximated by the function f_N:

$$f_N \;\; = \;\; C_{N1}\left[\ln\left(1 + C_{N2}N\right) + C_{N3}N\right] \qquad (18)$$
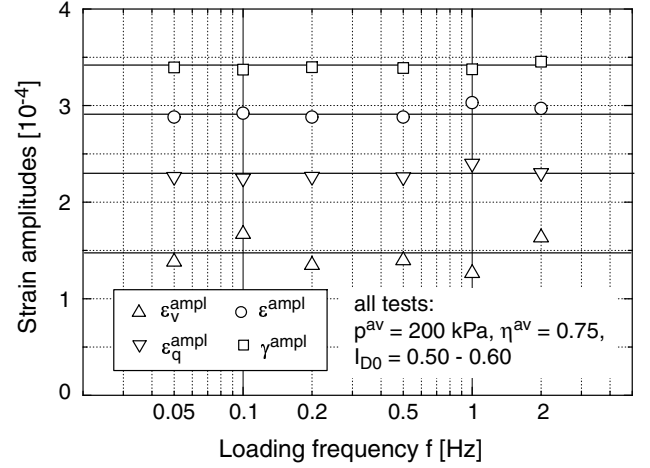
Fig. 25: Strain amplitudes as a function of the loading frequency f
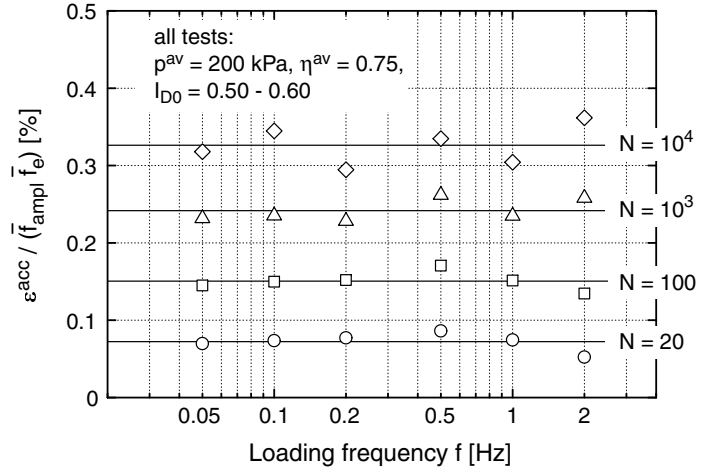
Fig. 26: Residual strain $\varepsilon^{\mathrm{acc}}/(\bar{f}_{\mathrm{ampl}}\, \bar{f}_e)$ for different loading frequencies f
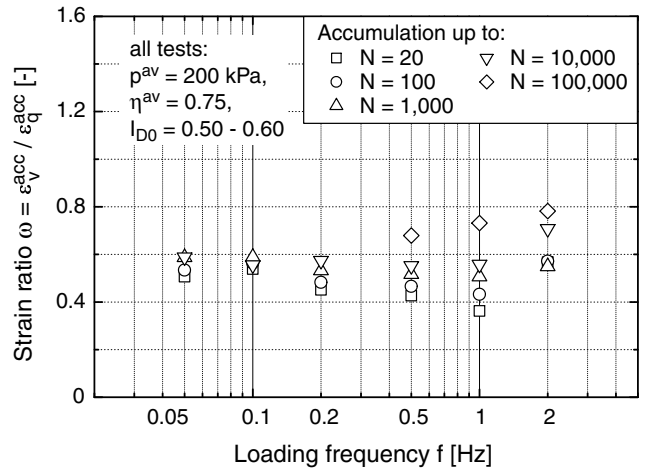
Fig. 27: Strain ratio ω versus loading frequency f

$$\dot{f}_N = \underbrace{\frac{C_{N1}C_{N2}}{1+C_{N2}N}}_{\dot{f}_N^A} + \underbrace{C_{N1}C_{N3}}_{\dot{f}_N^B} \qquad (19)$$

with the material constants $C_{N1} = 3.4 \cdot 10^{-4}$, $C_{N2} = 0.55$ and $C_{N3} = 6.0 \cdot 10^{-5}$. The function f_N consists of a logarithmic and a linear part. The logarithmic part is pre-dominant for $N < 10,000$ (see also Sawicki & Świdziński [12,13]), however, the linear part is necessary for the description of the accumulation at higher cycle numbers which is faster than logarithmic. The function f_N could be also fitted to the results of tests up to $N_{\max} = 2 \cdot 10^6$.
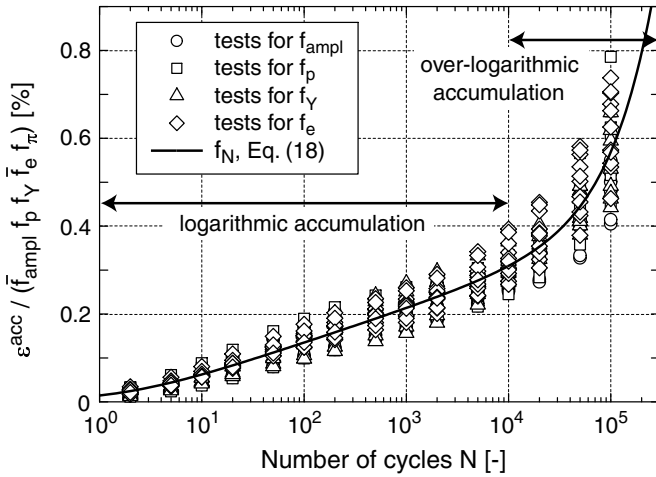
Fig. 28: Normalized accumulation curves

As already mentioned the number of cycles N alone is not a suitable state variable for the description of cyclic preloading. The amplitude of the previous cycles is also of importance. To simplify the matter the accumulation rate was splitted into a rate of structural accumulation ($\sim \dot{f}_N^A$) and a basic rate ($\sim \dot{f}_N^B$). $g^A = \int \dot{g}^A \, \mathrm{d}N = \int f_{\mathrm{ampl}} \dot{f}_N^A \, \mathrm{d}N$ is used as a state variable for cyclic preloading depending on $\varepsilon^{\mathrm{ampl}}$ and N. Replacing N in Eq. (19) by g^A one obtains

$$\dot{f}_N^A = C_{N1}C_{N2}\exp\left(-\frac{g^A}{C_{N1}\,f_{\mathrm{ampl}}}\right) \qquad (20)$$

The severe problem of the determination of cyclic preloading in situ is discussed by Triantafyllidis and Niemunis [26], Wichtmann and Triantafyllidis [27,28] and Triantafyllidis et al. [29].

11   Influence of the grain size distribution

The presented tests on the uniformly graded sand No. 1 (Fig. 4) are being supplemented by tests on the gradations 2 and 3 (Fig. 4), which have similar uniformity indices $1.4 \leq U = d_{60}/d_{10} \leq 1.9$ but different mean grain diameters $0.35 \text{ mm} \leq d_{50} \leq 1.45 \text{ mm}$. Also tests on the

well-graded sand No. 4 ($U = 4.5$, Fig. 4) are being conducted, which has a similar d_{50} compared to sand No. 1. Figure 29 presents the accumulation curves for an identical average stress, identical initial densities and similar strain amplitudes. The grain size distribution curve strongly affects the accumulation rate. An increase of $\dot{\varepsilon}^{\mathrm{acc}}$ with a decreasing mean diameter d_{50} at $U = \text{const}$ was found. At $d_{50} = \text{const}$ the intensity of accumulation significantly increases with U.

Up till now the presented accumulation model can describe the behaviour of all sands by simply modifying the material constants. The tests on different gradations will be carried on in future. We expect that based on those tests we will be able to simplify the model (some constants might become redundant) or at least to correlate most constants to the granular properties (grain size distribution, grain shape, content of fines).
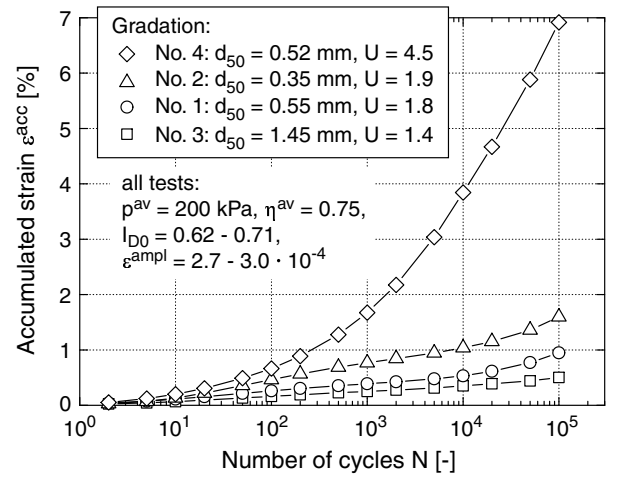
Fig. 29: Accumulation curves $\varepsilon^{\mathrm{acc}}(N)$ for different gradations

12   Summary, conclusions and outlook

In order to develop a high-cycle model for the accumulation of strain and/or stress in sand under cyclic loading numerous cyclic triaxial tests and cyclic multiaxial direct simple shear (CMDSS) tests were performed. This paper describes the model in brief and concentrates on the experimental results from the tests with triaxial compression and uniaxial stress cycles. The main conclusions from these tests are:

- The direction of accumulation (cyclic flow rule) does exclusively depend on the average stress ratio $\eta^{\mathrm{av}} = q^{\mathrm{av}}/p^{\mathrm{av}}$. A slight increase of the volumetric component of the direction of accumulation with the number of cycles N was observed.

- The direction of accumulation is in agreement with the flow rule of material models for monotonous

loading (modified Cam clay model, hypoplastic model).

- The accumulation rate is proportional to the square of the strain amplitude, $\dot{\varepsilon}^{\mathrm{acc}} \sim (\varepsilon^{\mathrm{ampl}})^2$, at least within the range of the tested amplitudes $0.5 \cdot 10^{-4} \leq \varepsilon^{\mathrm{ampl}} \leq 5 \cdot 10^{-4}$.

- Our triaxial tests contradict the so-called "common compaction curve" (Sawicki and Świdziński [12,13]).

- The accumulation rate $\dot{\varepsilon}^{\mathrm{acc}}$ increases with decreasing average mean pressure p^{av} and with increasing average stress ratio η^{av}.

- $\dot{\varepsilon}^{\mathrm{acc}}$ grows with increasing void ratio.

- $\dot{\varepsilon}^{\mathrm{acc}}$ does not depend on the loading frequency (0.05 Hz $\leq f \leq 2$ Hz).

- For $N > 10^4$ the accumulated strain $\varepsilon^{\mathrm{acc}}$ increases faster than the logarithm of the number of cycles N.

- The intensity of accumulation $\dot{\varepsilon}^{\mathrm{acc}}$ is strongly affected by cyclic preloading.

- The accumulation rate depends significantly on the grain size distribution curve. An increase of $\dot{\varepsilon}^{\mathrm{acc}}$ with a decreasing mean grain diameter d_{50} was found. A well-graded soil is compacted much faster than a poorly-graded one.

At present we are extending the model for triaxial extension. Furthermore, the influence of the polarization and the shape of the strain loop on the accumulation rate is being tested. Results of preliminary cyclic triaxial tests with varying stress loops in the p - q - plane (uniaxial paths with different inclinations as well as elliptic ones) and some CMDSS test data can be found in [3]. Also the boundaries of the validity of the explicit formulas have to be checked and extended in further experiments (e.g. it was found that the relationship $\dot{\varepsilon}^{\mathrm{acc}} \sim (\varepsilon^{\mathrm{ampl}})^2$ overestimates the accumulation for $\varepsilon^{\mathrm{ampl}} > 10^{-3}$). A correlation of the material constants of the accumulation model with the grain characteristics (grain size distribution, grain shape, content of fines) will be tried out.

Acknowledgements

References

[1] Mróz Z, Norris VA. Elastoplastic and Viscoplastic Constitutive Models for Soil with Application to Cyclic Loading. Soil Mechanics - Transient and Cyclic Loads. Constitutive Relations and Numerical Treatment, Pande GN, Zienkiewicz OC (eds.), John Wiley and Sons, 1982:173-218.

[2] Dafalias, YF. Bounding surface elastoplasticity-viscoplasticity for particulate cohesive media. Deformation and Failure of Granular Materials, Proceedings IUTAM Conf., Delft, 1982:97-107.

[3] Wichtmann T, Niemunis A, Triantafyllidis T. The effect of volumetric and out-of-phase cyclic loading on strain accumulation. Cyclic Behaviour of Soils and Liquefaction Phenomena, Proc. of CBS04, Bochum, March/April 2004, Balkema, 2004:247-56.

[4] Matsuoka H, Nakai T. A new failure for soils in three-dimensional stresses. Deformation and Failure of Granular Materials, Proc. IUTAM Symp. Delft, 1982:253-63.

[5] Lentz RW, Baladi GY. Simplified procedure to characterize permanent strain in sand subjected to cyclic loading. International Symposium on soils under cyclic and transient loading, 1980:89-95.

[6] Lentz RW, Baladi GY. Constitutive equation for permanent strain of sand subjected to cyclic loading. Transportation Research Record, 1981;810:50-54.

[7] Suiker ASJ. Static and cyclic loading experiments on non-cohesive granular materials. Report No. 1-99-DUT-1, TU Delft, 1999.

[8] Helm J, Laue J, Triantafyllidis T. Untersuchungen an der RUB zur Verformungsentwicklung von Böden unter zyklischen Belastungen. Beiträge zum Workshop: Boden unter fast zyklischer Belastung: Erfahrungen und Forschungsergebnisse, Institute of Soil Mechanics and Foundation Engineering, Ruhr-University Bochum, Issue No. 32, 2000:201-22.

[9] Gotschol A. Veränderlich elastisches und plastisches Verhalten nichtbindiger Böden und Schotter unter zyklisch-dynamischer Beanspruchung. PhD thesis, University Kassel, 2000.

[10] Youd TL. Compaction of sands by repeated shear straining. Journal of the Soil Mechanics and Foundations Division, ASCE, 1972;98(SM7):709-25.

[11] Silver ML, Seed HB. Volume changes in sands during cyclic loading. Journal of the Soil Mechanics and Foundations Division, ASCE, 1971;97(SM9):1171-82.

[12] Sawicki A, Świdziński W. Compaction curve as one of basic characteristics of granular soils. Proc. of 4th Colloque Franco-Polonais de Mechanique des Sols Appliquee, Grenoble, 1987;1:103-15.

[13] Sawicki A, Świdziński W. Mechanics of a sandy subsoil subjected to cyclic loadings. International Journal For Numerical And Analytical Methods in Geomechanics, 1989;13:511-29.

[14] Budhu M. Nonuniformities imposed by simple shear apparatus. Canadian Geotechnical Journal, 1984;20:125-37.

[15] Marr WA, Christian JT. Permanent displacements due to cyclic wave loading. Journal of the Geotechnical Engineering Division, ASCE, 1981;107(GT8):1129-49.

[16] Ko HY, Scott, RF. Deformation of sand in hydrostatic compression. Journal of the Soil Mechanics and Foundations Division, ASCE, 1967;93(SM3):137-56.

[17] Pyke R, Seed HB, Chan CK. Settlement of sands under multidirectional shaking. Journal of the Geotechnical Engineering Division, 1975;101(GT4):379-98.

[18] Ishihara K, Yamazaki F. Cyclic simple shear tests on saturated sand in multi-directional loading. Soils and Foundations, 1980;20(1):45-59.

[19] Yamada Y, Ishihara K. Yielding of loose sand in three-dimensional stress conditions. Soils and Foundations, 1982;22(3):15-31.

[20] Shenton MJ. Deformation of railway ballast under repeated loading conditions. Railroad track mechanics and technology, Pergamon Press, 1978:405-25.

[21] Kempfert HG, Gotschol A, Stöcker T. Kombiniert zyklische und dynamische Elementversuche zur Beschreibung des Kurz- und Langzeitverhaltens von Schotter und granularen Böden. Beiträge zum Workshop: Boden unter fast zyklischer Belastung: Erfahrungen und Forschungsergebnisse, Institute of Soil Mechanics and Foundation Engineering, Ruhr-University Bochum, Issue No. 32, 2000:241-54.

[22] Luong MP. Mechanical aspects and thermal effects of cohesionless soils under cyclic and transient loading. Proc. IUTAM Conf. on Deformation and Failure of Granular Materials, Delft, 1982:239-46.

[23] Chang CS, Whitman RV. Drained permanent deformation of sand due to cyclic loading. Journal of Geotechnical Engineering, ASCE, 1988;114(10):1164-80.

[24] Niemunis A. Extended hypoplastic models for soils. Habilitation. Institute of Soil Mechanics and Foundation Engineering, Ruhr-University Bochum, Issue No. 34, 2003.

[25] Niemunis A, Wichtmann T, Triantafyllidis T. Explicit accumulation model for cyclic loading. Cyclic Behaviour of Soils and Liquefaction Phenomena, Proc. of CBS04, Bochum, March/April 2004, Balkema, 2004:65-76.

[26] Triantafyllidis T, Niemunis A. Offene Fragen zur Modellierung des zyklischen Verhaltens von nicht-bindigen Böden. Beiträge zum Workshop: Boden unter fast zyklischer Belastung: Erfahrungen und Forschungsergebnisse, Institute of Soil Mechanics and Foundation Engineering, Ruhr-University Bochum, Issue No. 32, 2000:109-34.

[27] Wichtmann T, Triantafyllidis T. Influence of a cyclic and dynamic loading history on dynamic properties of dry sand, part I: cyclic and dynamic torsional prestraining. Soil Dynamics and Earthquake Engineering, 2004;24:127-47.

[28] Wichtmann T, Triantafyllidis T. Influence of a cyclic and dynamic loading history on dynamic properties of dry sand, part II: cyclic axial preloading. Soil Dynamics and Earthquake Engineering, accepted for publication.

[29] Triantafyllidis T, Wichtmann T, Niemunis A. On the determination of cyclic strain history. Cyclic Behaviour of Soils and Liquefaction Phenomena, Proc. of CBS04, Bochum, March/April 2004, Balkema, 2004:321-32.